Probe beam deflection studies of nanostructured catalyst materials for fuel cells†

G. García,[a] M. M. Bruno,[b] G. A. Planes,[b] J. L. Rodriguez,[a] C. A. Barbero*[b] and E. Pastor*[a]

Received 24th April 2008, Accepted 14th August 2008
First published as an Advance Article on the web 30th September 2008
DOI: 10.1039/b806938g

Probe beam deflection (PBD) techniques, both as cyclic voltadeflectometry (CVD) and chronodeflectometry (CD), were applied for the first time to the study of the electrochemistry of nanostructured Pt materials which are commonly used as electrocatalysts in fuel cells. The electrochemical surface reactions, including faradaic processes, double layer charging and specific anion adsorption were easily detected. Quantitative analysis of the chronodeflectometric data made possible to elucidate the dynamics of double layer charging in such materials and to determine the potential of zero charge (pzc) of the metal present either as a monolithic mesoporous material or as metal nanoparticles supported on carbon. The electro-oxidation of CO, adsorbed on nanostructured Pt, was also studied by CVD and CD being able to detect the formation of CO_2 and H_3O^+ related with the nucleation and growth process which controls the rate of CO stripping. The interplay of Pt oxide formation and CO_{ad} electrooxidation, both in potential and time, was detected indicating possible application of the technique to other electrocatalysts.

A. Introduction

The analysis of ion exchange processes at the electrode/electrolyte interface is of fundamental importance for the elucidation of the overall reaction mechanisms at the electrochemical interface. In this context, probe beam deflection (PBD) appears to be a promising method to study the reactions that take place at the catalysts surface in fuel cells and related systems. PBD is an optical *in situ* technique that allows monitoring the concentration profiles established at the electrode/electrolyte interface during the electrochemical reaction.[1–4] This concentration profile is generated by all mobile species produced/consumed at the electrode surface. Therefore, for a given geometrical pathlength, the flux rises significantly when the ratio between electrochemically active and geometrical area increases.[5] This increment can be easily achieved using nanostructured electrode materials where the active surface area is significantly higher than for compact electrodes. Such materials include mesoporous catalysts and those constituted by metal nanoparticles, usually supported on a conductive matrix (*e.g.* carbon). The electrochemical reactions occurring at those electrodes are quite relevant to technological applications like fuel cells,[6] batteries,[7] sensors,[8] supercapacitors[9] *etc*. Therefore, it is important to devise techniques able to study, directly or indirectly, the surface reactions on those novel materials.

PBD measurements on practical nanostructured electrodes can render information not easily accessed by other methods. In that sense, the monitoring of ion fluxes in the double layer region allows to directly determine the potential of zero charge (pzc) of solid electrodes which have been only measured indirectly from capacitance measurements. Using the PBD approach, the pzc of carbon materials has been successfully measured and compared to the value obtained by impedance spectroscopy.[10]

On the other hand, Pt-based catalysts used for anode fuel cell have the problem of continuous poisoning with the CO generated as impurity in the reforming process for hydrogen production or as intermediate formed in the dissociative adsorption of organic molecules.[11] For this reason, one of the most important research activities nowadays is the study of CO electro-oxidation and the development of catalysts that are more tolerant to the presence of small amounts of this gas.[12]

Recently, PBD has been applied to study the oxidation of adsorbed CO in saturated CO perchloric acid solution at a polycrystalline Pt electrode.[13] Gas production should involve a positive beam deflection as $\partial n/\partial c < 0$ for gases[14] and $\partial c/\partial z < 0$ (formation of CO_2 at the electrode surface). However, a negative value of Ψ was observed during oxidation of CO_{ad} to CO_2 in the presence of CO in the solution. These results were explained assuming that H_3O^+ formation, concurrent with CO_2 production, dominates the observed signal. Experiments in the absence of CO in the solution are still lacking for a better understanding of this reaction. Moreover, the possibility of testing by PBD the CO_{ad} oxidation on materials with

[a] *Departamento de Química Física, Universidad de la Laguna, 38071 Tenerife, Spain. E-mail: epastor@ull.es; Fax: +34 (0)922318002; Tel: +34 (0)922318028*
[b] *Departamento de Química, Universidad Nacional de Río Cuarto, 5800 Río Cuarto, Argentina*

† Electronic supplementary information (ESI) available: Figures of simulation and additional experimental data. See DOI: 10.1039/b806938g

applications for fuel cells and micro-fuel cells makes the technique even more interesting.

B. Experimental

All measurements were carried out at room temperature in an electrochemical cell using a three-electrode assembly. A high surface area carbon rod was used as counter electrode and a reversible hydrogen electrode (RHE) in the supporting electrolyte was employed as reference. All potentials in the text are referred to this electrode. Experiments were carried out in 1 M sulfuric acid and 1 M perchloric acid, prepared from high purity reagents (97% and 70%, respectively, Merck p.a.) and Milli-Q water (Millipore). The electrolyte was saturated with pure nitrogen (99.98%, Air Liquide) or CO gases (99.997%, Air Liquide), depending on the studies.

PBD set-up

The PBD arrangement has been described before.[6] Briefly, the system consists of a He–Ne laser (Uniphase model 1103P, 2 mW), a focusing lens (50 nm), the electrochemical cell (optical quartz recipient with a 2 cm optical path length) and a position-sensitive detector (UDT model PIN-LSC/SD). The laser beam is focused to a diameter of roughly 60 μm in front the planar electrode and aligned parallel to the electrode surface, with an initial beam diameter of 0.63 mm. It monitors the refractive index gradient correlated to the concentration gradient, by deflection according to the magnitude and sign of the refractive index gradient.[1] The diameter of the spot at the detector is about 4 mm, which is much smaller than the surface area of the latter. The position-sensitive detector is placed 25 cm behind the electrochemical cell, resulting in an effective sensibility of 1 μrad mV^{-1}. The point of zero deflection is established where no concentrations gradients are present at the electrode surface. The voltammetric and deflectometric signals are recorded, along with the potential, using a homemade program developed in a LabView (National Instruments) environment. The program controls a potentiostat (Amel 2049) trough an AD/DA card (AT-MIO, National Instruments). Cyclic voltadeflectograms (CVDs) were recorded simultaneously with the corresponding cyclic voltammograms (CVs). The chronodeflectograms (CDs) were recorded simultaneously with the corresponding chronoamperograms (CAs).

PBD detects the concentration profiles generated by all mobile species produced/consumed at the electrode surface. Each component (i) contributes to the beam deflection Ψ according to:

$$\Psi = \frac{w}{n}\sum_i \frac{\partial n_i}{\partial c_i}\frac{\partial c_i}{\partial z} \qquad (1)$$

where w is the interaction pathlength of the probe beam with the electrode, n the refractive index of the electrolyte, c_i the concentration of each i species and z the distance to the surface. Eqn (1) is an approximation for an infinitely thin laser beam and for small deflections.[1] With w/n and $\partial n/\partial c$ constant in a given experiment, a positive beam deflection Ψ results for a positive $\partial c/\partial z$ *i.e.* when the surface concentration is lower than the bulk concentration, and *vice versa* for a negative beam deflection. While cyclic voltadeflectrograms render qualitative information on the ion fluxes, chronodeflectograms are more open to a quantitative interpretation.[15] Specifically, CD data could be directly related to the population of ions at the electrode surface allowing the calculation of double layer parameters like the pzc.

For a potential pulse driving an instantaneous or discontinuous process, like charging–discharging a double layer, the experimental CD signal (Ψ) follows eqn (2):[16]

$$\Psi(x,t) = \left(w\frac{\partial n}{\partial C}\right)\frac{Cs}{\sqrt{\pi D_0 t}}\frac{x}{2D_0 t}e^{-x^2/4D_0 t} \qquad (2)$$

where Cs is the effective (taking into account the surface area) concentration of ions exchanged on the electrode surface, D_0 is the diffusion coefficient of the mobile species, x is the beam–electrode distance, w is the beam pathlength and $\partial n/\partial C$ is the change of refractive index with concentration for the mobile species.

Note that the refractive index does not appear in eqn (2) because it is considered the refraction of the beam when it leaves the cell. Using eqn (2) and suitable parameters it is possible to simulate the experimental chonodeflectometric data. The simulation is performed writing the equations into spreadsheet software (Excel®).

By differentiation of eqn (2) as a function of x, it can be shown that the time to reach the maximum PBD signal (t_{max}), in a discontinuous process, is equal to:[1,16]

$$t_{max} = \frac{x^2}{6D_0} \qquad (3)$$

Reinserting eqn (3) into eqn (2) renders the relationship of the maximum PBD signal with the ion surface concentration, which is a function of the electrode potential, for a fixed beam to electrode distance (x):

$$\Psi(E)_{x,t_{max}} = \left(w\frac{\partial n}{\partial C}\right)\left(\frac{6^{3/2}e^{-3/2}}{2\sqrt{\pi}x^2}\right)Cs(E) \qquad (4)$$

Therefore, the changes of ion surface concentration with potential [$Cs(E)$] could be evaluated by measuring the maximum PBD signal [$\Psi(E)$] when the electrode potential is pulsed from a fixed initial potential to various potentials.

Electrode preparation and electrochemical characterization of MP-Pt and NPtC catalysts

The mesoporous Pt (MP-Pt) working electrode was prepared following the procedure previously described.[17] The catalyst was obtained by electrochemical reduction of a mixture of aqueous hexachloroplatinic acid (8%) and octaethyleneglycol monohexadecyl ether ($C_{16}EO_8$) (50% weight fraction) onto a gold surface at 60 °C and 0.15 V. Then, the electrode was washed by leaving it in distilled water, which is replaced completely each 2 h, during 48 h.

In the studies of the nanostructured Pt/C catalyst (NPtC), the working electrode was a commercial Pt/C catalyst (20 wt% metal/C, ETEK) which consisted in Pt nanoparticles (3 nm diameter) supported on carbon microparticles, deposited from

a suspension as a thin layer over a gold surface. An aqueous suspension of 4.0 mg ml^{-1} of the NPtC catalyst was prepared by ultrasonically dispersing it in 15 μl of Nafion (5 wt% Aldrich) and pure water. An aliquot of the dispersed suspension was pipetted on the gold surface and dried at ambient temperature.[4]

The quality of the catalysts was characterized recording the CVs in the supporting electrolyte solution at a scan rate of 0.015 V s^{-1}.

CO stripping voltammograms were obtained after bubbling this gas in the cell for 10 min at 0.25 V, followed by nitrogen purging to remove the excess of CO and scanning the potential in the positive direction.

C. Results and discussion

PBD study of electrochemical surface reactions in 1 M $HClO_4$

First, CVD measurements of the Pt surface were performed in a electrolyte solution where negligible adsorption of the electrolyte ions occur. With this purpose, MP–Pt electrode and commercial NPtC catalyst were studied in 1 M $HClO_4$. Similar results were obtained for both materials, only those for MP–Pt will be shown.

The profile for a MP–Pt in 1 M $HClO_4$ (see ESI,† Fig. S1) resembles those described in the literature for flat or slightly roughened Pt electrodes.[18,19]

In principle, the features in the CVD can be interpreted in terms of the production and consumption of protons at the Pt interface.[20] The following reactions have to be considered:

• 0.05–0.40 V: hydrogen adsorption/desorption region:

$$Pt\text{–}(H) + H_2O \rightleftarrows Pt + H_3O^+ + e^- \quad (5)$$

• 0.40–0.75 V: double layer region, where water and hydroxyl ions adsorb on the surface without faradaic transfer, but electron-transfer occurs at $E > 0.60\ V_{RHE}$ corresponding to the onset of the reaction:[21]

$$Pt + 2H_2O \rightleftarrows Pt\text{–}(OH) + H_3O^+ + e^- \quad (6)$$

• $E > 0.75$ V: platinum oxide formation:

$$Pt\text{–}(OH) + H_2O \rightleftarrows Pt\text{–}O + H_3O^+ + e^- \quad (7)$$

During the positive potential scan, reactions (5), (6) and (7) take place to the right and the probe beam deflects toward the electrode surface due to the production of protons, increasing the acid concentration next to the electrode surface and causing a negative beam deflection. Thus, a sharp decrease occurs from 0.05 to 0.50 V where the highest proton production takes place. Then, the signal increases as the diffusion of protons from the surface is the prevailing process, and finally diminishes again when the adsorption of hydroxyl ions and oxide formation begin. Conversely, the change of Ψ with the potential turns positive (deflection away the electrode surface) during the reverse potential scan, where protons are consumed and the curve describes just the opposite behaviour than in the positive sweep.

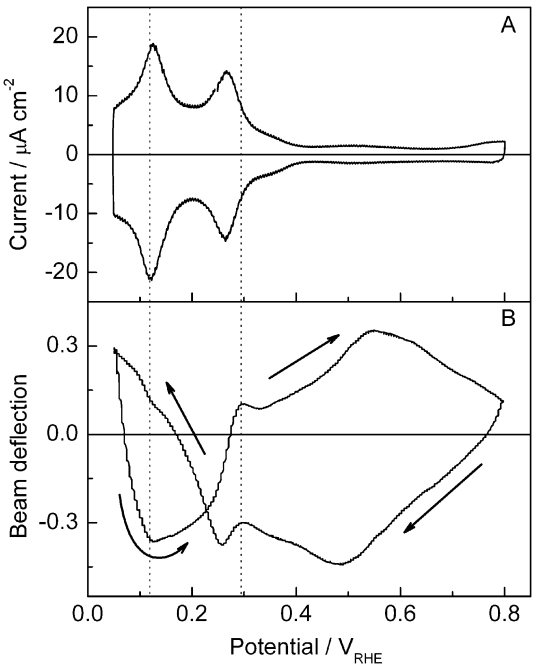

Fig. 1 CV (A) and CVD (B) of MP–Pt in 1 M H_2SO_4. $\nu = 0.015$ V s^{-1}.

PBD study of the electrochemical surface reactions in 1 M H_2SO_4

In a second step, CVDs experiments were performed in an electrolyte where specific anion adsorption on Pt has been shown to take place,[22] that is 1 M H_2SO_4, to see if the technique is able to detect such surface process.

Fig. 1 shows the CV and CVD curves for a MP-Pt electrode in 1 M H_2SO_4. The CV is similar to that previously reported for MP-Pt in the same electrolyte[6] and displays features resembling the CV obtained in 1 M $HClO_4$. However, the CVD is strikingly different to that measured in perchloric acid and seems to contain more information than the CV.

The results can be analyzed as follows:

• $0.05 < E < 0.40$ V: in Fig. 1B, during the positive-going potential scan in the range 0.05–0.125 V, the probe beam deflects toward the electrode surface indicating hydrogen desorption [eqn (5)]. Afterwards, a positive change of Ψ with the potential occurs between 0.125 and 0.30 V, indicating a deflection away from the electrode surface (just at the same potential than the first H_{ad} desorption peak in the CV). This results can be interpreted assuming that the H_{ad} desorption is not the sole reaction that happens in this potential range, but the adsorption/desorption of sulfate species (HSO_4^-/SO_4^{2-}). The change of sign in the CVD signal suggests that the pzc is located in this region, but it has to be considered that the CVD signal depends strongly on the scan rate and initial potential. Therefore, the exact location of the pzc in that region will be established from chronodeflectometry, where such effects are not present (see below).

On the other hand, the following equilibrium reactions take place in solution:

$$H_2SO_4 + H_2O \rightleftarrows HSO_4^- + H_3O^+ \quad (8)$$

$$HSO_4^- + H_2O \rightleftarrows SO_4^{2-} + H_3O^+ \quad (9)$$

Gain of HSO_4^- and loss of SO_4^{2-} in the solution happen next to the surface when increasing the potentials positively,[23] caused by the formation of H_3O^+ in surface reactions (5) and (6). Accordingly, the consequent deflectogram in this potential range can not be deduced only in terms of proton production/consumption, but the result of the coexisting processes, each one contributing to the net concentration gradient and deflection. Therefore, it is concluded that the positive deflection between 0.125 and 0.30 V in Fig. 2B is related mainly with the adsorption of anions. In the reverse potential scan, the CVD curve continuously increases for $E < 0.27$ V but a change in the slope is apparent at 0.125 V, the same potential for the change in the positive-going sweep.

The response between 0.25 and 0.32 V in Fig. 2B requires special attention. At *ca.* 0.30 V in the positive and reverse potential scans, a clear peak is defined in the deflection curve. The peak coincides with the potential of desorption of strongly adsorbed H atoms. It is likely that desorption of H is coupled with adsorption of bisulfate ions because it occurs at potentials positive to pzc. The anion concentration depletion is shown as a positive deflection signal. On the other hand the signal due to desorption of strongly adsorbed H occurs at potentials negative to the pzc and is dominated by H^+ formation. Such an interpretation is supported by the fact that the peak is not seen in $HClO_4$ where no specific anion adsorption occurs.

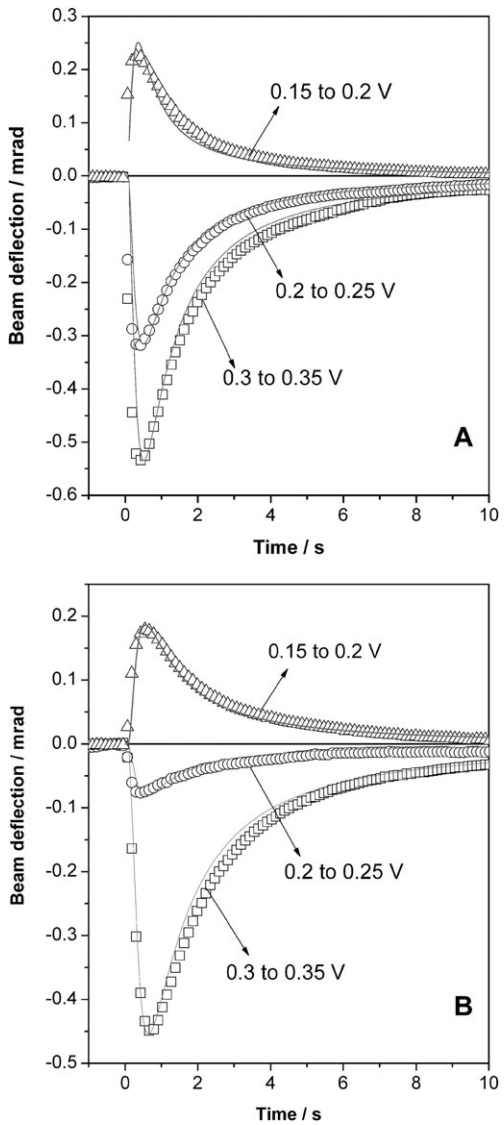

Fig. 2 Chronodeflectometric profiles measured while stepping the electrode potential between the values described in the figures. Electrolyte = 1 M H_2SO_4. (A) MP-Pt electrode, (B) NPtC electrode. The grey lines show the profiles simulated using eqn (2) and appropriate parameters.

• $0.40 < E < 0.75$ V: In the double layer region, a charged solid is in contact with the liquid phase, consisting of solvent molecules, ions and dipolar species, which become organized near the solid surface under the orienting force of the static electric field. As mentioned before, the adsorption of bisulfate goes through a maximum at 0.40 V and that of sulfate at 0.70 V. In the positive-going potential run, the deflection increases between 0.33 and 0.55 V indicating that adsorption of bisulfate species prevails. After that, in the 0.55–0.80 V range, the metal surface is more positively charged and the conversion of adsorbed bisulfate to adsorbed sulfate occurs, generating protons at the surface (eqn (9))[20] and producing a decrease in the PBD signal. Moreover, the electron donor character of water enhances and reaction (7) takes place, also producing protons which are responsible for the decrease in Ψ. The explanations for the shape of the CVD in the negative scan direction in this potential range are similar to those given before but assuming the consumption of protons and the adsorption of bisulfate. A measurement taken between 0.35 and 0.80 V shows clearly only the feature due to anion adsorption (see ESI,† Fig. S2). The absence of these features in perchloric media confirms that they have to be related to the presence of adsorbed anions.

It is important to select an appropriate potential window for the clear definition of CVD features. When the scanning window is extended to include the region of oxide formation/reduction (see ESI,† Fig. S3) some features change.

During the positive-going potential scan, a strong diminution in the deflection is recorded at $E > 0.75$ V, corresponding to the Pt oxide formation. Accordingly, in the negative potential run, the change in Ψ with the potential turns positive which is indicative of the Pt oxide reduction.

The incursion in the PtO region disturbs the CVD at lower potentials due to the strong deflection signals developed. In the reported data in the literature,[1,19,20] the electrodes were usually scanned up to 1.50 V and the details in the double layer region, and even in the H_{ad} region, were obscured.

The results suggest that porous metallic electrodes are highly suitable to study the process occurring at the electrode surface using PBD techniques.

Determination of pzc on nanostructured Pt electrodes by chronodeflectometry

Using chronodeflectometry it is possible to estimate the changes in concentration of mobile species at the electrode surface. Typical chronodeflectometric responses, obtained using a MP-Pt electrode in 1 M H_2SO_4 are shown in Fig. 2A. As it can be seen, the sign of the CD signal changes when the potential is stepped around 0.2 V.

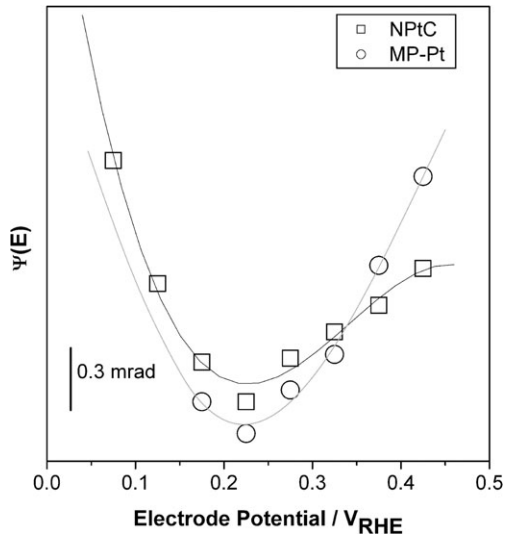

Fig. 3 Dependence of $\Psi(E)$, calculated from pulses as depicted in Fig. 2, for MP-Pt (circles, gray line) and NPtC (squares, black line). All points were measured in 1 M H_2SO_4.

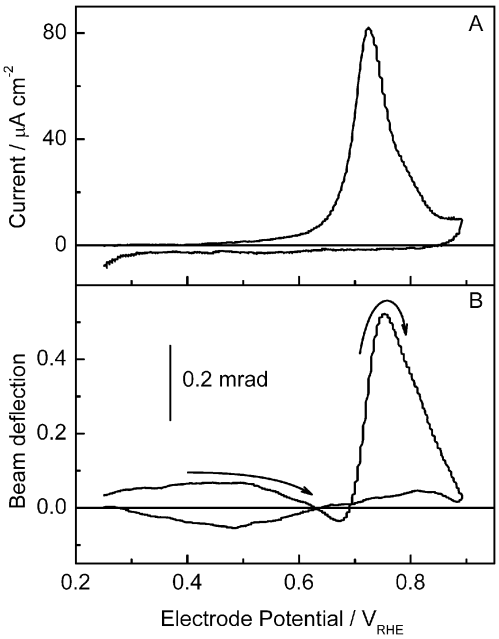

Fig. 4 CV (A) and CVD (B) for CO_{ad} oxidation in 1 M H_2SO_4 at MP-Pt. $v = 0.015$ V s^{-1}.

A similar behaviour is observed for CD measurements performed at NPtC electrodes in the same electrolyte (Fig. 2B). The chrono-deflectometric profiles were simulated using eqn (2). The general parameters used in the simulation were: $D_0 = 2.6 \times 10^{-5}$ cm^2 s^{-1} (sulfuric acid binary electrolyte[24]), partial $dn/dC = 0.011$.[1] The concentration of active sites (Cs) and the beam–electrode distance were different for each electrode. Accordingly $Cs = 1.62 \times 10^{-3}$ mol cm^{-3} and $x = 96$ μm were used for NPtC (Fig. 2B) and $Cs = 4.26 \times 10^{-3}$ mol cm^{-3} and $x = 90$ μm were employed for MP-Pt (Fig. 2A).

The good fitting (see also ESI,† Fig. S4 and S5) indicates that the double layer charging occurs in a negligible time compared with the CD measurement. While such assumption is obvious for a double layer charging of a flat electrode, and also for a nanoparticulated system, it is not always the case in porous materials. It has been shown that double layer charging of a monolithic mesoporous carbon material occurs as a continuous process due to restricted diffusion.[1] Therefore, the internal checking of the fitting is necessary to allow the use of eqn (3) to measure $Cs(E)$ in the calculation of the pzc.

The quantitative analysis of CD data, described in the experimental part, allows the estimation of the changes of the surface concentration with potential from the pulses described in Fig. 2. To simplify the interpretation, the integral variation between an initial potential and different final potentials is estimated (Fig. 3). In that way, the PBD signal will be proportional to the amount of ion exchanged from the initial potential to the final potential. If the potentials are stepped inside the double layer region, the ions exchanged will correspond to the changes in the ion population inside the double layer. At potentials more negative than the pzc, the amount of cations will decrease when the potential is stepped in the positive direction while at potentials positive to the pzc the amount of anions will increase for the same potential step. At the pzc, the curve should show a minimum.[25]

As can be seen, while they have some differences, the profiles obtained in both electrodes reveal a minimum value at *ca.* 0.22 ± 0.05 V. This value corresponds to the potential of zero charge of Pt in the media and it agrees reasonably with the value reported in the literature, for flat polycrystalline electrodes, of 0.20 V.[26] It has been reported that the pzc of Pt nanoparticles shifts up to 35 mV when the size of the particles is decreased from 30 to 1 nm.[27] While it is obvious that MP-Pt and NPtC present Pt of different sizes, electronic effects causing the shift of pzc are more likely to occur at small particle sizes below 10–15 nm.[28] However, we did not find differences between both electrode materials because the shift would be below the precision range of the measurements (0.05 V which is the potential step used to measure it).

PBD study of CO adsorption/desorption

Once shown the ability of the technique to detect the adsorption of species at the electrode surface, we studied the oxidation of CO at both MP-Pt and NPtC electrodes.

CO_{ad} oxidation on MP-Pt electrodes. PBD techniques are specially suited to study faradaic processes involving adsorbed or immobilized intermediates since these species do not contribute directly to the overall signal, making the interpretation easier (only ionic species and dissolved gases have influence on the deflectrometric signals).

The reaction for the electro-oxidation of adsorbed CO can be written as:

$$Pt\text{–}CO + Pt\text{–}(OH) + H_2O \rightarrow CO_2 + H_3O^+ + 2Pt + e^- \quad (10)$$

In the reaction, only CO_2 and H_3O^+ could be detected by PBD since surface species (Pt–OH and Pt–CO) do not change the refractive index of the solution (the large value of the water self-diffusion coefficient makes the corresponding profiles negligible at the experimental values of beam–electrode distances). In ref. 13 the authors assumed that CO interacts

directly with water and reactions (6), (7) and (10) occur simultaneously. However, we considered that CO can be oxidized only once Pt–(OH) is formed.

In our experiments, the peak potential for CO_{ad} electro-oxidation in the CV is located at 0.72 for MP-Pt with an onset potential at 0.50–0.55 V (Fig. 4A). This value resembles those from previous works.[13,18]

Fig. 4B shows the corresponding signal for the probe beam deflection during CO stripping. In the positive potential scan, at $E > 0.50$ V the deflection decreases, indicating that reaction (6) takes place. Subsequently, a sharp change in the deflection occurs at 0.67, increasing Ψ up to a maximum at 0.75 V for MP-Pt. In this potential region reactions (6), (7) and (10) coexist, but the production of CO_2 in the last one seems to determine the net sign of the PBD. This could be due to the fact that $\partial n/\partial c$ for CO_2 is negative and larger[1] than $\partial n/\partial c$ for H_3O^+. Note that the peak potential in PBD is shifted due to the time delay between the surface reaction and the detection at the laser at several (50–100 μm) away.

Our results seem to be in contradiction to those presented by Shi *et al.*,[13] where a decrease in the beam deflection was recorded for CO_{ad} oxidation at Pt(pc) in CO-saturated perchloric acid. However, it has to be mentioned that in the present paper a different experimental set-up (PBD is not commercially available and in our case is not combined with reflectance measurements) and a lower scan rate have been used for CO_{ad} oxidation in the absence of CO in solution (careful removal of CO from the solution assures that only CO_{ads} is oxidized). The conjunction of these changes could facilitate the acquisition of PBD predicted curves for the production of CO_2 gas which implies a positive deflection. In the back scan, no current is observed due to complete removal of CO by oxidation.

Accordingly, the PBD signal only shows the feature due to anion desorption at less positive potentials. Finally, a decrease in the beam deflection is observed above 0.75, indicating that the production of CO_2 is diminishing (by the consumption of the CO_{ad} monolayer) and reaction (7), that produces protons at the electrode surface, prevails.

When the initial coverage of CO is lower than in the experiment described in Fig. 4, the signal due to OH adsorption and oxide formation is more apparent in the CVD but the CV remains the same, albeit with smaller charge (see ESI,† Fig. S6), pointing out the usefulness of the PBD technique for studying oxidation of adsorbed species.

CO_{ad} oxidation on NPtC electrodes. The peak potential for CO_{ad} electro-oxidation is located at 0.80 V for commercial NPtC (Fig. 5A), as previously reported.[29] Fig. 5B displays the CVD obtained for the stripping of CO on NPtC, where a similar behaviour to that of MP-Pt is established. Thus, the deflection decreases for $E > 0.5$ during the upward scan and suddenly increases from 0.72 V attaining a peak at 0.86 V. The same explanation proposed for MP-Pt applies in this case. Again, the results are in contradiction to those presented by Shi *et al.*[13] As in Fig. 4, a decrease in the beam deflection is observed above 0.86 V, coinciding with the decrease in CO_2 formation.

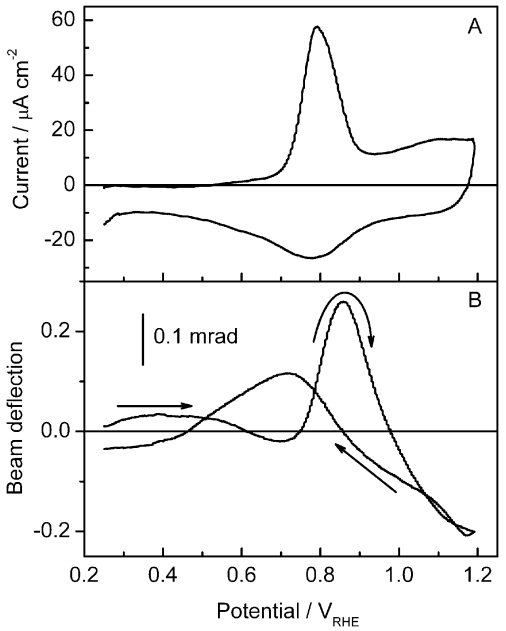

Fig. 5 CV (A) and CVD (B) for CO_{ads} oxidation in 1 M H_2SO_4 at NPtC (ETEK). $v = 0.015$ V s^{-1}.

In the back scan, a small current is observed in Fig. 5A due to the reduction of Pt oxide formed in the positive-going run at potentials more positive than 0.95 V. Accordingly, the PBD signal, measured during the back scan, shows a deflection increase due to proton consumption during oxide reduction describing a clear positive peak at *ca.* 0.72 V followed by the feature due to anion desorption at less positive potentials.

It is noteworthy that, while the deflectometric signal is dominated by CO_2 formation, fluxes due to reaction (6) are also detected in the CVDs depicted in Fig. 4 and 5. This discrimination ability is likely to be due to the small potential window where the CO stripping occurs, and should allow the study of CO poisoning on reaction (6) at different electrode materials.

Dynamic effects in CO_{ads} oxidation

Previous studies on the electrochemical oxidation of CO adsorbed on MP-Pt electrodes using chronoamperometry has shown that the oxidation follows a profile typical of a nucleation and growth process.[30] The characteristic curve describes a broad current maximum after the initial current spike has decayed. Such a feature is clearly seen during the oxidation of CO previously adsorbed on MP-Pt (Fig. 6A).

Since PBD is a technique nearly as fast as electrochemistry, in contrast with other techniques like *in situ* FTIR, such dynamic effects can be easily studied. As is displayed in Fig. 6B, the nucleation step (denoted by a sharp current spike) is correlated with a small negative deflection peak. The broad current feature is related to a broad positive deflection peak. Using the same interpretation we have proposed for the CVD profiles, the negative deflection is related with the proton expulsion due to Pt oxide formation [eqn (7)] being, in the best of our knowledge, the first time that direct evidence of this reaction has been observed.

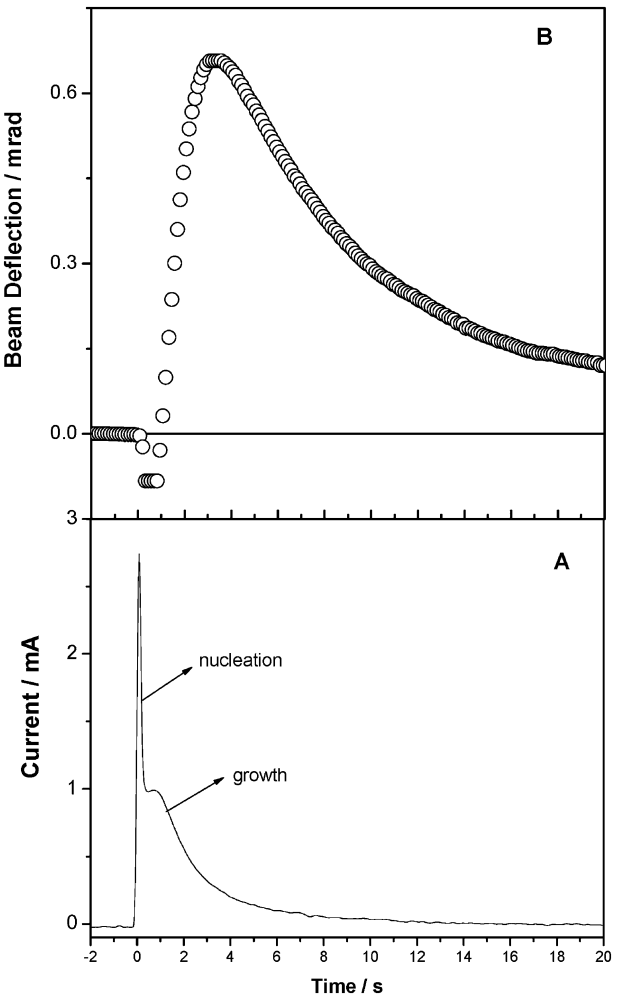

Fig. 6 Chonoamperometric (A) and chronodeflectometric (B) profiles of a MP-Pt electrode fully covered by adsorbed CO during oxidation to CO_2. The potential is stepped from the equilibrium adsoption potential of 0.25 to 0.80 V where all CO is oxidized. The electrolyte is 1 M H_2SO_4.

On the other hand, the positive deflection peak corresponds to CO_2 formation (solute concentration increases with negative partial dn/dC) due to CO_{ad} oxidation. Therefore, it is likely that the fast oxide formation occurs with nucleation in specific catalytic sites while the CO_{ad} oxidation happens through reaction (10) reducing the oxide and its electrochemical regeneration is responsible for the slow "growth" process.

The results gives direct evidence in support to the early proposition by McCallum and Pletcher[31] that CO oxidation rate is determined by the rate of nucleation and growth of oxide islands in the CO monolayer at a polycrystalline platinum electrode. An alternative view, but also in agreement with our data, was proposed by Lebedeva *et al*. to explain CO oxidation on stepped Pt single crystals in sulfuric media.[32] They describe the oxidation of CO by a nucleation of the CO oxidation reaction at defects sites (*i.e*. steps) and a growth mechanism due to a fast CO diffusion from less reactive places (*i.e*. terraces) to step sites.

Conversely, it has been suggested that the oxidation of the CO adlayer requires the completion of at least two different processes:[33,34] oxidative desorption of CO and re-establishment of the double layer involving (bi)sulfate anion adsorption on the CO-free platinum surface. The PBD data presented here do not support such mechanism as a building up of the double layer will imply a positive deflection (bisulfate anion depletion in front of the electrode) as it is observed for a clean Pt electrode (Fig. 1) while both in CD and CVD negative deflection is detected before the onset of CO_{ads} oxidation.

The small pre-peak could also be due to a time delay between different fluxes, as it has been described before in other systems.[35,36] To clarify this point, the chronodeflectometric signal in Fig. 6 was simulated (Fig. 7) taking into account the contributions due to CO_2 and H_3O^+, which are produced during CO_{ad} oxidation in reaction (10). For this simulation, CD profiles plot were calculated as the addition of two PBD signals [eqn (1)], where each PBD profile obeyed eqn (2), with the parameters of each mobile species. As CO_2 is uncharged, no migration effects have to be considered and the electrolyte remains binary. The diffusion coefficient of proton used was that of the binary electrolyte (2.6×10^{-5} cm^2 s^{-1}),[24,25] while the diffusion coefficient of CO_2 was 2.2×10^{-5} cm^2/s.[37] The beam electrode distance was 176 μm, the partial dn/dC of H_3O^+/HSO_4^- was 0.011 and that of CO_2 was 0.014.[38] As it can be seen, a good fitting of the whole curve is obtained assuming a multicomponent flux. Therefore, the fluxes observed are only slightly dominated by the CO_2 flux and the CD technique is able to separate the contribution.

It is noteworthy that the plot contains features which can only be explained by a multicomponent flux. First of all, the pre-peak (see insert in Fig. 7) has to be related to a multicomponent flux. Additionally, if the beam-electrode distance is

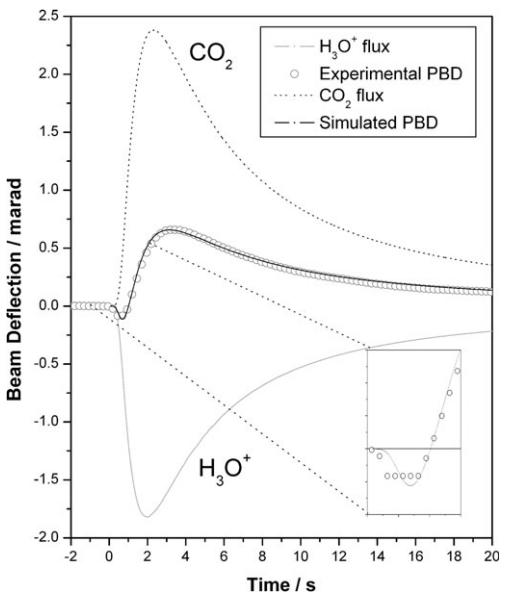

Fig. 7 Comparison of the experimental (open circles) chronodeflectometric profiles depicted in Fig. 6 with the simulation of fluxes due to H^+ and CO_2, according to eqn (2), which are added according to eqn (1). The grey full line corresponds to the contribution of H_3O^+ while the black dotted line corresponds to the contribution of CO_2. The full black line describes the overall flux. In the insert the region of the pre-peak is expanded.

calculated from the maxima in the PBD signal using eqn (3), a value of 226 μm is obtained, which is away from the true value of 176 μm. Finally, the magnitude is almost half the one expected for a flux of only one species. Therefore, the CD profile contains data which unambiguously lead to the reaction mechanism.

On the other hand, the shape of the CD in Fig. 7 could help to explain the results described in ref. 15. If CVD measurements are performed at relatively high scan rates, the signal detected should corresponds to the response at short times in Fig. 7, which is the region of the pre-peak where negative deflection is recorded. It is clear that CD measurements reveal a more accurate picture of the actual ion exchange processes than CVD.

Conclusions

In summary, results in the present paper prove that PBD can monitor the flux of ionic and gaseous products to and from the electrode interface of high surface area Pt materials. The technique is sensitive to faradaic surface process (*e.g.* oxide formation), double layer charging, specific adsorption of anions and CO_{ad} oxidation. The specific adsorption of sulfate species on Pt is clearly observed. Additionally, the determination of the pzc was realized by the quantitative analysis of the chronodeflectometric profiles. While the technique detects overall fluxes, it has been shown that using potential (in cyclic voltadeflectrograms) or time (in chronodeflectograms) allows to separate different fluxes in multicomponent systems.

Both the formation of CO_2 and the production of H_3O^+ are detected during the electro-oxidation of CO_{ad}. The capability of fast measurement provides direct evidence of CO_2 and H_3O^+ formation during the nucleation and growth process leading to electro-oxidation of CO_{ad}.

In that way, PBD has demonstrated to be an appropriate technique for the evaluation of the electrochemical interface of nanostructured Pt catalysts, both mesoporous Pt and Pt nanoparticles supported on carbon. The results permit to improve the understanding of some important mechanistic aspects of their interface processes. It has to be considered that both materials are practically used in low temperature fuel cells, where alternative *in situ* techniques for testing the catalysts are not readily available.

Since the technique is able to detect independently oxide formation and CO oxidation (Fig. 4), it should be useful to study CO poisoning on alloy electrode materials where another metal (*e.g.* Ru), which form oxides at lower potentials, is added to oxidize the adsorbed CO. The same promise holds for the study of other ways to avoid CO poisoning such as oxidant (*e.g.* O_2) introduction. In that case, changes in the mechanism of adsorbed CO oxidation could be detected by monitoring the ratio of H^+ to CO_2 produced, using chronodeflectometry (see Fig. 7).

On the other hand, the effect of higher temperatures on CO poisoning seems difficult to be studied using PBD due to the interference of thermal gradients in the measurement.

Acknowledgements

C. A. Barbero and G. A. Planes are permanent research fellows of CONICET. M. M. Bruno thanks CONICET for a graduate fellowship. The work was financed by MEC (MAT2005-06669-C03-02, NAN2004-09333-C05-04, FEDER, SPAIN) and SECYT-UNRC (PDMA), CONICET (PIP5201), FONCYT (PICTR03-453), ARGENTINA). The authors acknowledged the financing by AECI of the collaboration project (PCI A/4233/05 and A/5301/06).

References

1 C. A. Barbero, *Phys. Chem. Chem. Phys.*, 2005, **7**, 1885.
2 C. Barbero and M. C. Miras, in *Tecnicas deflectometricas aplicadas al estudio de procesos electroquimicos, in Electroquimica y Electrocatalisis*, ed. Nicolas Alonso-Vante, e-libro net, Buenos Aires, 2nd edn, 2003.
3 J. D. Rudnicki, F. R. McLarnon and E. J. Cairns, in *Techniques for Characterization of Electrodes and Electrochemical Processes*, ed. R. Varma and J. R. Selman, Plenum, New York, 1991.
4 C. Barbero, M. C. Miras, R. Koetz and O. Haas, *Solid State Ionics*, 1993, **60**, 167.
5 C. A. Barbero and M. C. Miras, *J. Argent. Chem. Soc.*, 2003, **91**, 1–40.
6 K. W. Lux and K. J. Rodríguez, *Nano Lett.*, 2006, **6**, 288–295.
7 H. Yamada, K. Tagawa, M. Komatsu, I. Moriguchi and T. Kudo, *J. Phys. Chem. C*, 2007, **111**, 8397–8402.
8 L. Lu and A. Eychmüller, *Acc. Chem. Res.*, 2008, **41**, 244–253.
9 J. M. Elliott and J. R. Owen, *Phys. Chem. Chem. Phys.*, 2000, **2**, 5653–5659.
10 M. M. Bruno, N. G. Cotella, M. C. Miras and C. A. Barbero, *Chem. Commun.*, 2005, 5896–5898.
11 S. Park, Y. Xie and M. J. Weaver, *Langmuir*, 2002, **18**, 5792–5798.
12 G. García, J. A. Silva-Chong, O. Guillén-Villafuerte, J. L. Rodríguez, E. R. González and E. Pastor, *Catal. Today*, 2006, **116**, 415.
13 P. Shi, I. Fromondi, Q. Shi, Z. Wang and D. A. Scherson, *Anal. Chem.*, 2007, **79**, 202.
14 R. Mehra, *Proc. Indian Acad. Sci. (Chzem. Sci.)*, 2003, **115**, 147–154.
15 F. Garay and C. A. Barbero, *Anal. Chem.*, 2006, **78**, 6733–6739.
16 C. Barbero, M. C. Miras and R. Koetz, *Electrochim. Acta*, 1992, **37**, 429.
17 G. Planes, G. García and E. Pastor, *Electrochem. Commun.*, 2007, **9**, 839.
18 V. Kertész, G. Inzelt, C. Barbero, R. Kötz and O. Haas, *J. Electroanal. Chem.*, 1995, **392**, 91.
19 E. D. Bidoia, F. McLarnon and E. J. Cairns, *J. Electroanal. Chem.*, 2000, **482**, 75.
20 R. Kötz, C. Barbero and O. Haas, *Ber. Bunsen-Ges. Phys. Chem.*, 1993, **97**, 427.
21 J. M. Orts, R. Gómez, J. M. Feliu, A. Aldaz and J. Clavilier, *Electrochim. Acta*, 1994, **39**, 1519.
22 S. Thomas, Y.-E. Sung, H. S. Kim and A. Wieckowski, *J. Phys. Chem.*, 1996, **100**, 11726–1735 and refs therein.
23 T. Iwasita and F. C. Nart, *J. Electroanal. Chem.*, 1990, **295**, 215.
24 J. M. Nzikou, M. Baklouti, L.-M. Vincent and F. Lapicque, *Chemical Engineering and Processing*, 1997, **36**, 161–165.
25 G. A. Planes, M. C. Miras and C. A. Barbero, *Chem. Commun.*, 2005, 2146–2148.
26 M. E. Martins, *J. Argent. Chem. Soc.*, 2005, **93**, 143–153.
27 K. J. J. Mayrhofer, B. B. Blizanac, M. Arenz, V. R. Stamenkovic, P. N. Ross and N. M. Markovic, *J. Phys. Chem. B*, 2005, **109**, 14433.
28 K. Dick, T. Dhanasekaran, Z. Zhang and D. Meisel, *J. Am. Chem. Soc.*, 2002, **124**, 2312.
29 J. Xi, J. Wang, L. Yu, X. Qiu and L. Chen, *Chem. Commun.*, 2007, 1656–1658.
30 J. Jiang and A. Kucernak, *J. Electroanal. Chem.*, 2002, **533**, 153–165.

31 C. McCallum and D. Pletcher, *J. Electroanal. Chem.*, 1976, **70**, 277.
32 N. P. Lebedeva, M. T. M. Koper, J. M. Feliu and R. A. van Santen, *J. Electroanal. Chem.*, 2002, **242**, 524–525.
33 J. M. Orts, E. Louis, L. M. Sander and J. Clavilier, *Electrochim. Acta*, 1998, **44**, 1221.
34 J. M. Feliu, J. M. Orts, R. Gomez, A. Aldaz and J. Clavilier, *J. Electroanal. Chem.*, 1994, **372**, 265.
35 D. E. Grumelli, A. Wolosiuk, E. Forzani, G. A. Planes, C. Barbero and E. J. Calvo, *Chem. Commun.*, 2003, 3014–3015.
36 D. E. Grumelli, F. Garay, C. A. Barbero and E. J. Calvo, *J. Phys. Chem. B*, 2006, **110**, 15345–15352.
37 A. Tamimi, Edward B. Rinker and Orville C. Sandall, *J. Chem. Eng. Data*, 1994, 330–332.
38 R. N. O'Brien, private communication, 1994.